Improving efficiency of multi-phase cascaded DC-DC boost converters in discontinuous conduction mode suitable for renewable energy application

Arwindra Rizqiawan, Muhammad Farras Muzakki, Jihad Furqani
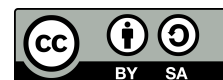School of Electrical Engineering and Informatics, Institut Teknologi Bandung, Bandung, Indonesia

Article Info

ABSTRACT

This study presents an improvement on the efficiency of a proposed multiphase cascaded DC-DC boost converter by employing discontinuous conduction mode (DCM) for its operation. The proposed multiphase cascaded DC-DC boost converter is characterized by high voltage gain and low input current ripple. This converter consists of two stages and is designed to connect a photovoltaic (PV) system to a DC microgrid bus. First, the loss equations for the converter are analyzed, then discontinuous conduction mode is applied to the first stage of the proposed converter by adjusting the second stage output current value, which represents grid load fluctuations. Subsequently, the efficiency of the proposed converter will be evaluated. Further, comparison with two operation modes, continuous conduction mode (CCM) and boundary conduction mode (BCM), is provided. To verify the proposed analysis and calculation, experiments are conducted by implementing the circuitry in a lab-scale prototype. The results show that by implementing DCM operation, the proposed converter achieves the highest efficiency of 92.2% at an output power of 120 W, while other modes achieve lower efficiencies as in CCM with 90.17% at an output power of 215.5 W. In the proposed converter, the dominant source of losses is attributed to the inductor, accounting for approximately 62% of the total losses in DCM. The operation of DCM has demonstrated a substantial reduction in switching losses, leading to a notable increase in efficiency.

Corresponding Author:

Arwindra Rizqiawan
School of Electrical Engineering and Informatics, Institut Teknologi Bandung
Ganesha 10 St., Bandung, Indonesia
Email: windra@itb.ac.id

NOMENCLATURE

V_o	: Output voltage (V)	T_S	: Switching period (s)
V_{in}	: Input voltage (V)	F_S	: Switching frequency (Hz)
V_Q	: Switch voltage drop (V)	Δi_L	: Inductor current ripple (A)
V_c	: Capacitor voltage (V)	M_a	: Voltage gain
i_L	: Inductor current (A)	R_{load}	: Load resistance (Ω)
R_L	: Inductor resistance (Ω)	P_L	: Inductor conduction/winding loss (W)
R_Q	: Switch resistance (Ω)	P_{cl}	: Core inductor loss (W)
L	: Inductance (H)	$R_{L,DC}$	: DC resistance of inductor (Ω)

i_o	: Output current (A)	$R_{L,AC}$	: AC resistance of inductor (Ω)
R_D	: Diode resistance (Ω)	ΔB, B	: Inductor core's flux density (T)
V_D	: Diode voltage drop (V)	A_e	: Cross-section area (cm^2)
D	: Duty cycle	N	: Number of inductor cores
D_A	: Duty cycle of first-stage converter	a, b, c, d	: Core material constant
D_B	: Duty cycle of second-stage converter	E	: Maximum input voltage (V)
D_a	: Duty cycle during charging	P_D	: Diode conduction loss (W)
D_b	: Duty cycle during discharging	P_Q	: Switch conduction loss (W)
D_c	: Duty cycle during zero current	P_S	: Switching loss (W)

1. INTRODUCTION

The utilization of photovoltaic (PV) as a source of electrical energy is increasingly widespread due to its clean nature. PV systems are flexible and can be installed in urban areas as well as solar power plants. In urban areas, PV systems can be installed on rooftops, as described in [1], [2]. PV can also be installed in areas with limited access to electricity [3], [4]. On the other hand, Indonesia has many remote areas that are difficult to connect [5], [6]. To meet the needs and electrify these areas, PV utilization connected to residential homes can be done through a DC microgrid system [7], [8]. The utilization of PV connected to a DC microgrid encounters several issues, such as the very low DC output voltage from PV. The typical output voltage of PV ranges from 18 to 36 V. On the other hand, the bus voltage of the DC microgrid is around 325-400 V [9]–[11]. To achieve the microgrid voltage, PV panels can be connected in series to increase the output voltage. However, this solution potentially reduces the overall performance of PV due to partial shading conditions that cause PV to produce current equivalent to the panel with the least amount of light intensity [12]. A practical solution to overcome this voltage issue is to utilize power electronic devices that can boost the PV output voltage to match the bus voltage of the DC microgrid.

The device that can amplify the DC output voltage is a boost converter. Considering the need to connect PV to the microgrid, a high voltage gain is required, ranging from 7 to 10 times. However, conventional DC-DC boost converters can only achieve voltage gains up to 5 times [13]. The solution to this problem is to cascade or stack multiple converters together [14], [15]. This configuration offers higher voltage gain with good efficiency [16], [17]. Utilizing a capacitor or inductor to achieve a high-gain converter has also been reported [18], [19]. Another issue with PV penetration in a microgrid is the susceptibility of PV to current ripple. This current ripple causes significant power losses in PV [20]. A multiphase converter configuration can eliminate current ripples by adjusting the duty cycle according to the number of converter phases [21]. The input current ripple issue can be addressed by using a multiphase configuration in the input section of the converter. The mentioned converters are able to achieve high-gain output but not necessarily obtain low current ripple [22], yet multiphase converters are able to achieve zero current ripple but only in a specific duty cycle, thus the gain is sacrificed. In accordance with the specified criteria, the multiphase cascaded DC-DC boost converter emerges as a viable solution due to its capacity to deliver a substantial voltage increase while minimizing input current ripple. This topology features a two-stage configuration, commencing with a multiphase setup in the first stage, subsequently interconnected in a series or cascaded manner with a boost converter in the second stage. However, it should be noted that the efficiency of the multiphase cascaded DC-DC boost converter has not reached its optimum state. As reported in [22], the converter's efficiency was enhanced to 89.19% through the optimization of inductance values and operation in boundary conduction mode (BCM). Furthermore, a laboratory prototype of the cascaded boost converter, designed for photovoltaic integration, demonstrated an efficiency of up to 96% at input voltage levels of 48 V, under CCM operation, as indicated in [23], at specific power points.

The objective here is to attain a highly efficient multiphase cascaded DC-DC boost converter while retaining its capability for substantial voltage amplification and minimal input current ripple, as highlighted in [22]. The analytical findings suggest a potential for increased efficiency in the converter's operation at designated power levels, alongside a notable reduction in switching losses in discontinuous conduction mode (DCM). In DCM, it is observed that there are no transient current situations at the switch, resulting in an absence of power dissipation during switching, ideally rendering switching losses negligible. This event can be described as zero current switching (ZCS) [24]. This observation prompts further investigation to ascertain the operational conditions that yield the highest efficiency while preserving the converter's distinctive attributes. Further, comparison with two operation modes, continuous conduction mode (CCM) and boundary conduction mode (BCM), is provided. Each converter parameter and its efficiency are analyzed in various converter con-

duction modes as in [25]. This research aims to analyze and increase the converter's efficiency by operating it in DCM.

This paper is structured as follows: i) Section 1 provides an introduction; ii) Section 2 discusses the topology of the proposed converter operation in discontinuous conduction mode; iii) Section 3 presents comparative evaluation of the proposed converter in various conduction modes, supported by simulation results using software and calculations; iv) Section 4 addresses experimental verification; and v) Section 5 presents the conclusions.

2.   MULTIPHASE CASCADED BOOST CONVERTER

The proposed converter consists of two stages. The first stage is a three-phase boost converter. This multiphase configuration is used to reduce input current ripple, and with a specific duty cycle configuration, the current ripple can be minimized or even eliminated [22]. The first stage converter is connected in series with a conventional boost converter in the second stage, as depicted in Figure 1. The cascaded configuration increases the voltage gain of the converter. These two converter stages are separated by capacitor C1, which acts as a buffer to enable the semi-independent operation of both stages.

2.1.   Converter operation in DCM

In order to evaluate the efficiency, it is essential to derive the equation that accounts for the losses occurring in the converter. These losses are obtained from the voltage gain equation. Components in the converter, such as diodes, switches, and inductors, possess parasitic elements represented by resistance R. The parasitic components introduce voltage drops across the elements, resulting in a non-ideal output voltage of the converter, which can be expressed in (1).

$$
\begin{aligned}
V_o = \ & \left(\frac{3D_A{}^2 V_{in}{}^2}{(1-D_B)\,2L_A F_s i_{L,B}} + \frac{V_{in}}{(1-D_B)} \right) - V_{in}{}^2 \left(\frac{3D_A{}^3 \left(R_{L,A} + R_{Q,A} - 2R_{D,A} \right)}{(1-D_B)\,4L_A{}^2 F_s{}^2 i_{L,B}} \right) \\
& - \frac{D_A V_{in} \left(R_{L,A} + R_{D,A} \right)}{(1-D_B)\,2L_A F_s i_{L,B}} - \frac{3D_A{}^2 V_{in} V_{Q,A}}{(1-D_B)\,2L_A i_{L,B}} - \frac{V_{D,A}}{(1-D_B)} - \frac{V_{Q,B} D_B + V_{D,B}(1-D_B)}{(1-D_B)} \\
& - \frac{R_{L,B} + R_{S,B} D_B + R_{D,B}(1-D_B)}{(1-D_B)^2} i_o
\end{aligned}
\tag{1}
$$

The (1) represents the non-ideal output voltage of the cascaded 3-1 phase boost converter in DCM. The voltage gain in BCM and CCM is similar, where there's only a single type of duty cycle function that exists. In DCM operation, the RMS value of the inductor current differs from CCM due to the presence of a time interval when the inductor current becomes zero ($D_c.T_S$). The RMS value of the current can be expressed in (2) and (3).

$$
i_{L,rms} = \sqrt{i_L{}^2 + \frac{\Delta i_L{}^2 (1+2D_c)}{12}}
\tag{2}
$$

$$
D_c = 1 - D_a \frac{M_A}{M_A - 1}
\tag{3}
$$

M_A represents the voltage gain of the converter. The value of DC depends on the rate at which the inductor discharges current, meaning that DC is dependent on MA under DCM operation. Therefore, the RMS value of the inductor current is also influenced by the voltage gain of the converter. The value of M_A is obtained from the voltage gain of the ideal DCM-operating boost converter, specifically in the case of a three-phase boost converter, as in (4).

$$
M_A = \frac{V_{C1}}{V_{in}} = \left(\frac{1 + \sqrt{1 + \frac{6D_a{}^2 . R_{Load}}{L_A . D_B . f_s}}}{2} \right)
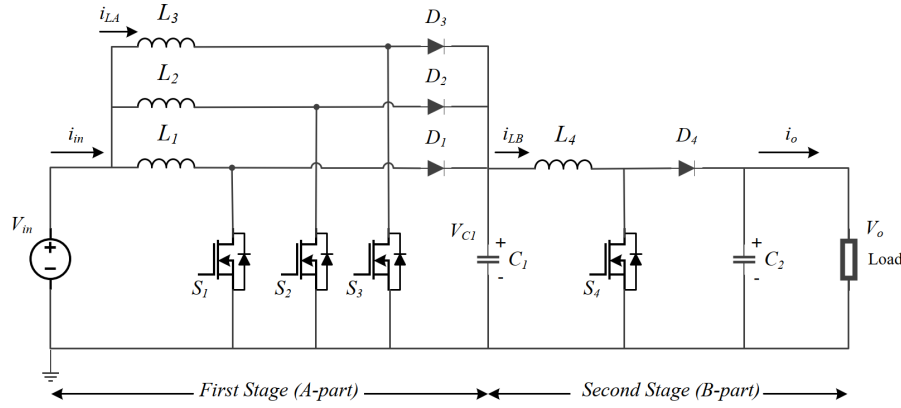\tag{4}
$$

Figure 1. Proposed converter topology

2.2. Losses analysis

The derivation of the voltage gain and efficiency equation of a multiphase cascaded DC-DC boost converter under CCM has been previously addressed in [22]. The calculation of conduction losses in DCM is similar to CCM, but there are slight differences in the switching loss. The complete formulation of the converter losses consists of inductor losses, diode conduction losses, switch conduction losses, and switching losses.

Power losses in the inductor originate from the winding and core of the inductor. In the winding of the inductor, there is copper resistance that results in AC and DC losses. The DC resistance of the inductor arises from the inherent resistance of the copper material, which is determined by the specific resistance of copper and the cross-sectional area of the winding wire. The AC resistance of the inductor occurs due to the skin effect phenomenon during high-frequency switching processes. As the switching frequency increases, the AC resistance also increases. The conduction losses in the inductor are formulated by (5) and (6).

$$P_{LA} = 3 \left(i_{L,A,rms}^2 . R_{L,A,DC} + \frac{\Delta i_{L,A}^2 . (1 + 2D_c)}{12} R_{L,A,AC} \right) \tag{5}$$

$$P_{LB} = i_{L,B,rms}^2 . R_{L,B,DC} + \frac{\Delta i_{LB}^2}{12} R_{L,B,AC} \tag{6}$$

Furthermore, the core losses of the inductor are proportional to the area of the hysteresis curve of the core material. The core losses of the inductor are a function of the peak-to-peak value of the magnetic flux density and the switching frequency of the converter. The value of the magnetic flux density can be calculated using (7).

$$\Delta B \approx \frac{E_{peak} . \left(\frac{D}{F_S} \right) . 10^8}{A_e . N} = \frac{L_A \Delta i_L . 10^8}{A_e . N} \tag{7}$$

To obtain the equation for core losses, it is necessary to know the type of core material used. In this study, the authors used powder-coated iron cores and sendust toroidal cores. The equation for core losses of these materials is obtained from the material datasheet [26] as in (8).

$$P_{cl} = n_L V \left(\frac{f}{\frac{a}{B^3} + \frac{b}{B^{2.3}} + \frac{c}{B^{1.65}}} + \left(dF_S^2 B^2 \right) \right) \tag{8}$$

Conduction losses in diodes and switches occur due to the resistance and internal voltage drop when the diodes are in the conducting state. These losses are determined by the RMS current flowing through the boost converter inductor. Conduction losses in diodes can be represented by (9) and (10).

$$P_{D,A} = 3 \left(i_{L,A,rms}^2 . R_{D,A} . D_b + V_{D,A} . i_{L,A} . D_b \right) \tag{9}$$

$$P_{D,B} = i_{L,B,rms}^2 . R_{D,B} . D_B + V_{D,B} . i_{L,B} . D_B \tag{10}$$

Conduction losses in switches can be represented by (11) and (12).

$$P_{Q,A} = 3\left(i_{L,A,rms}{}^2.R_{Q,A}.\,D_a +\ V_{Q,A}.i_A.D_a\ \right) \tag{11}$$

$$P_{Q,B} = i_{L,B,rms}{}^2.R_{Q,B}.\,D_B +\ V_{Q,B}.\,i_{L,B}.D_B \tag{12}$$

In [27], the switching losses have been formulated, which are not influenced by the operating voltage and the number of phases. However, when observing the transition from the on to off state, vice versa. In a switch, this process results in power losses due to non-spontaneous condition changes. In modern switching devices, such as wide-band gap switches, there is the possibility of additional losses due to oscillation during the switching transient [28]. Additionally, there are losses caused by the reverse recovery process in the diode within the switch. Therefore, the switching power losses can be expressed as in (13) and (14).

$$P_{S,A} = 3(E_{OFF,A}.i_{S,A,\ rms}.F_{S,A}) \tag{13}$$

$$P_{S,B} = (E_{ON,B}.i_{S,B,\ rms} + E_{ON,A}.i_{S,B,\ rms}).F_{S,B} \tag{14}$$

The value of E_{ON} represents the power loss when the switch transitions from off to on. The value of E_{OFF} represents the power loss when the switch transitions from on to off. It can be observed that in a boost converter switch, there are no switching losses from off to on. This is because in DCM condition, the inductor current is zero when the switch is turned on. Thus, a zero current switching (ZCS) process occurs, and the switching losses from on to off can be neglected.

3. COMPARATIVE EVALUATION FOR DIFFERENT CONDUCTION MODES
3.1. Converter conduction modes

The proposed converter can operate in various modes, namely continuous (CCM), boundary (BCM), and discontinuous (DCM) modes [29]. These operating modes are characterized by the behavior of the inductor current. The explanation will refer to Figure 2. In CCM, the inductor current always remains above zero. In other words, during both charging and discharging cycles, there is always a continuous current flowing through the inductor. In BCM, the behavior of the inductor current is similar to CCM. However, during the discharging cycle, the inductor current momentarily becomes zero. In the DCM, the shape of the inductor current is slightly different. There are three zones of current that occur in the inductor: charging, discharging, and zero current. The operation mode of the boost converter is influenced by several parameters within the converter. The boundary point is determined by the inductance, switching frequency, duty cycle, and output current [29]. In this study, the converter's operating mode will be determined by the output current, which represents the fluctuations in the grid load. In CCM and BCM modes, the inductor waveforms share a similar pattern, allowing the utilization of a single duty cycle notation. Therefore, the formulas applied are the same for both conduction modes. A comparison of the converter equations when operating in CCM and BCM, as detailed in [16], is summarized in Table 1.

Table 1. Converter formulas in BCM and CCM

| Aspect	Expression
Non-ideal output voltage	$V_o = \dfrac{V_{in}-V_{Q,A}D_A-V_{D,A}(1-D_A)}{(1-D_A)(1-D_B)} - \dfrac{R_{L,A}+R_{Q,A}D_A+R_{D,A}(1-D_A)}{3(1-D_A)^2(1-D_B)^2}i_o - \dfrac{V_{Q,B}D_B+V_{D,B}(1-D_B)}{(1-D_B)} - \dfrac{R_{L,B}+R_{Q,B}D_B+R_{D,B}(1-D_B)}{(1-D_B)^2}i_o$
Voltage gain	$M_A = \dfrac{V_o}{V_{in}} = \dfrac{1}{(1-D)^2} - \dfrac{R_{L,A}-3R_{L,B}(1-D)^2}{3(1-D)^4}i_o$
Inductor conduction loss	$P_{L,A} = \dfrac{R_{L,A,DC}}{3(1-D_A)^2(1-D_B)^2}i_o{}^2 + \dfrac{3\Delta i_{L,A}{}^2}{12}R_{L,A,AC}$ $P_{L,B} = \dfrac{R_{L,B,DC}}{(1-D_B)^2}i_o{}^2 + \dfrac{\Delta i_{L,B}{}^2}{12}R_{L,B,AC}$
Switch conduction loss	$P_{Q,A} = \dfrac{V_{Q,A}D_A}{(1-D_A)(1-D_B)}i_o + \dfrac{R_{S,A}D_A}{3(1-D_A)^2(1-D_B)^2}i_o{}^2$ $P_{Q,B} = \dfrac{V_{Q,B}D_B}{(1-D_B)}i_o + \dfrac{R_{Q,B}D_B}{(1-D_B)^2}i_o{}^2$
Diode conduction loss	$P_{D,A} = \dfrac{V_{D,A}}{(1-D_B)}i_o + \dfrac{R_{D,A}}{3(1-D_A)(1-D_B)^2}i_o{}^2$ $P_{D,B} = V_{D,B}i_o + \dfrac{R_{D,B}}{(1-D_B)}i_o{}^2$
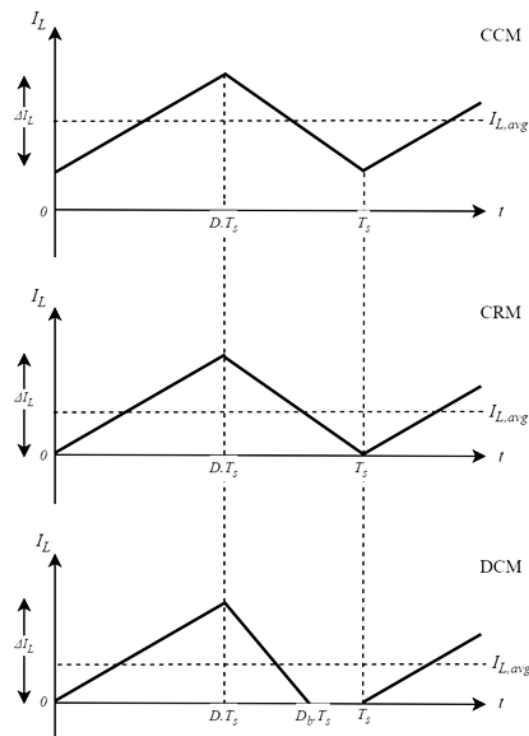
Figure 2. Inductor current at various conduction modes

3.2. Simulation verification

The converter circuit was implemented using PSIM 12.2 software for simulation purposes. The simulations were conducted to determine the boundary points for specific output currents based on predetermined component parameters. Additionally, the simulations aimed to observe the inductor current profiles in each operating mode of the converter. The model of the cascade multiphase DC-DC boost converter was designed to resemble real circuit phenomena, incorporating thermal loss and conduction loss components.

The input voltage of 36 V represents the output voltage of a photovoltaic system. The simulation control utilized pulse width modulation (PWM) signals to regulate the switches with specific duty cycles. A duty cycle value of 0.67 for the first stage of the converter has been previously tested in [22] for the same converter configuration, demonstrating the highest efficiency. The duty cycle for the second stage was set to 0.75 to achieve high voltage amplification. The switching frequency was set to 20 kHz. The chosen frequency value is based on achieving the highest efficiency while aligning with the converter's features, as optimized in [16]. Furthermore, the application of a 20 kHz frequency is commonly utilized in renewable energy, as indicated in [30]. In the first-stage, there's a phase delay of 120° to accommodate the three-phase circuit configuration.

The simulation results of the inductor current are shown in Figure 3. For the predetermined parameters, an output current of 0.32 A operates the converter in boundary mode. At this boundary point, the converter operates at a power of 150 W. The shape of the inductor current can be observed in the three operating modes as depicted in Figure 3. It can also be seen that the inductor current waveform is slightly distorted, especially at the charging and discharging edges. This distortion is caused by the parasitic components present in the simulated inductor.

3.3. Efficiency analysis

The derivation of the non-ideal output voltage, current, and power loss formulas for the converter has been performed in section 2. Subsequently, these formulas were input into data processing software to calculate the losses in each component of the converter and its overall efficiency. In addition to calculating the efficiency value, the calculation results also serve to determine the parameter values to ensure they do not exceed the converter's specifications during testing.

The output current used in the calculations consists of experimental data and several crucial data points. The lower limit of the calculation is set at an output current of 0.285 A, at which the converter operates in DCM mode. This value serves as the lower limit because, in addition to being in DCM, the converter's output voltage is already approaching its maximum allowable voltage of 450 V. Furthermore, the output current values are tested for each operating mode of the converter. The lower limit of the calculation is set at an output current of 1 A because at 1.2 A, the input current exceeds 12 A and goes beyond the converter's specifications. The efficiency trend for different output currents and power values is depicted in Figure 4.

It can be observed that efficiency decreases as the converter's power increases. In other words, in CCM, the efficiency decreases. This is because at higher power levels, the losses in the converter's components also increase. These losses are proportional to the increase in converter power. Additionally, in DCM, soft switching occurs, resulting in a significant reduction in switch losses. This is what leads to a notable increase in efficiency between BCM and DCM, despite being at similar output power levels. The loss characteristics of BCM and CCM are similar, hence the similarity in their loss calculations. Furthermore, the efficiency trends obtained from these calculations will be verified by comparing them with experimental results.
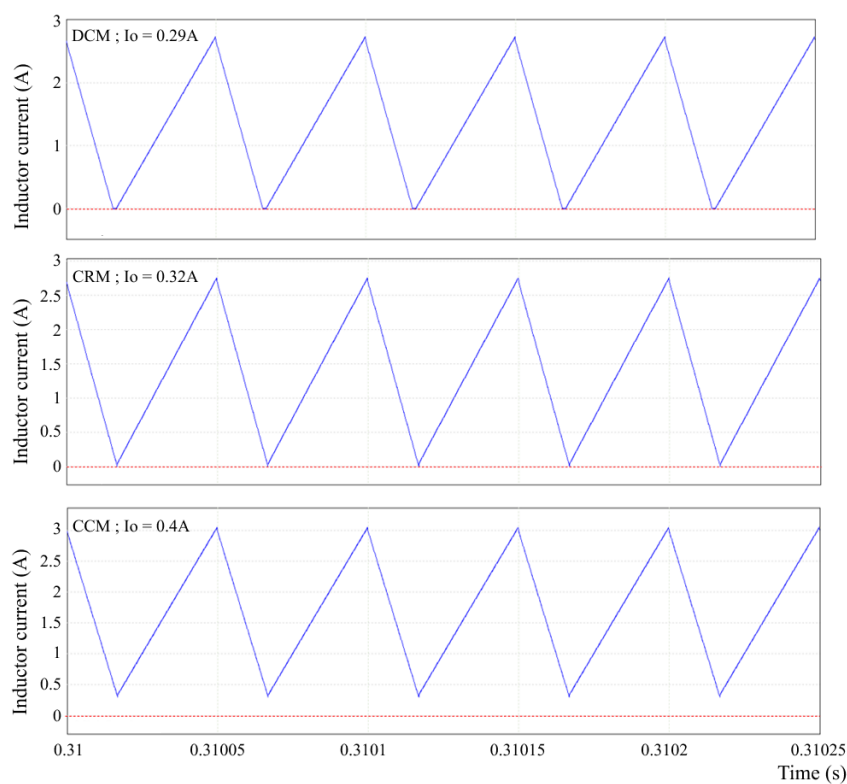

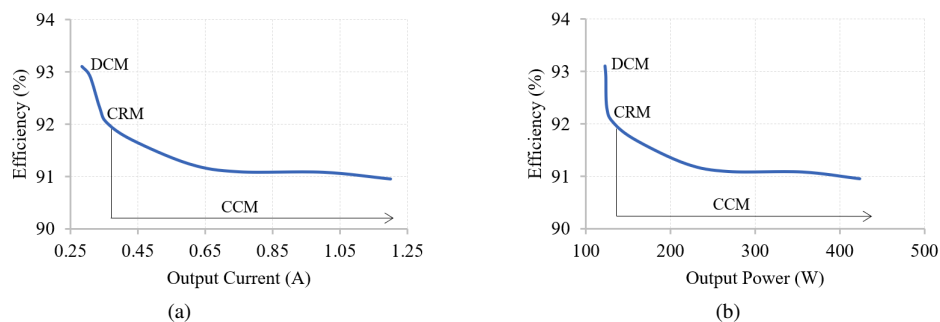Figure 3. Simulation result of inductor currents

Figure 4. Calculation results: (a) efficiency-output current and (b) efficiency-output power

4. EXPERIMENTAL VERIFICATION

4.1. Converter specification and setup

The experiments were conducted to observe the real phenomena of the multiphase cascaded DC-DC boost converter circuit and to verify the calculations performed. The circuit shown in Figure 1 was implemented with the addition of control circuitry and connected to measurement instruments such as an oscilloscope and power meter. The input DC voltage was adjustable from a rectifier circuit connected to a 3-phase transformer and LC filter. The converter output was connected to a variable resistor as the load. The experimental circuit arrangement is shown in Figure 5, and the converter's parameters are described in Table 2.
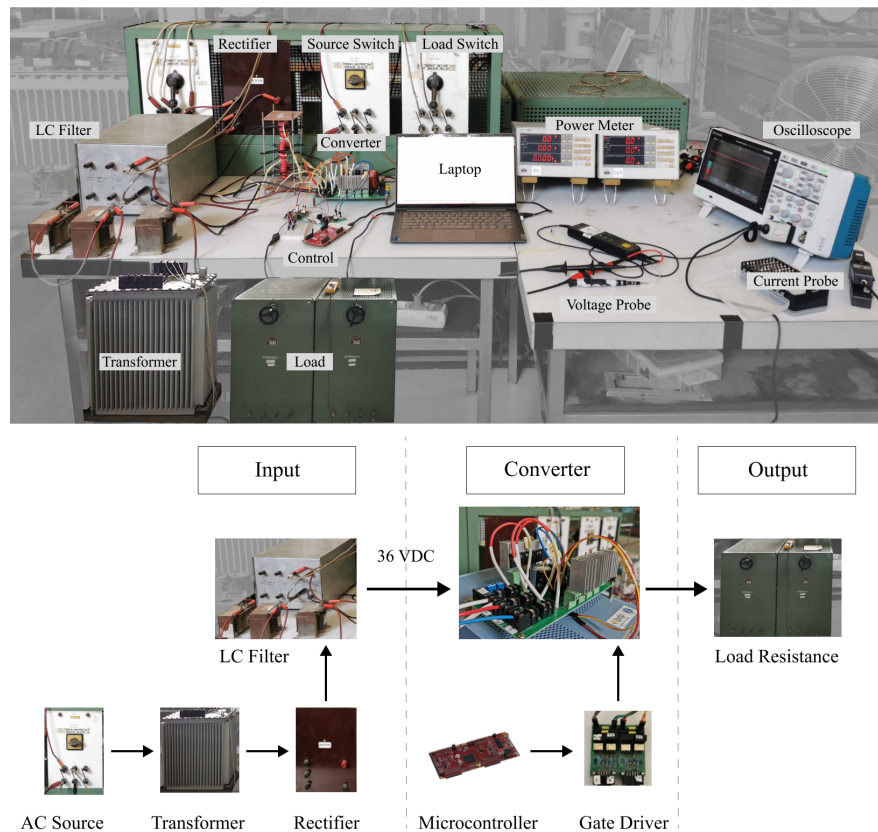
Figure 5. Experiment setup

Table 2. Converter parameters and components

Parameter	Value	Parameter	Value
DC input voltage	36 V	Duty cycle	0.67 and 0.75
DC output voltage	350 – 450 V	Inductor (L_1-L_3)	0.435 mH
Maximum power rated	400 W	Inductor (L_4)	2.5 mH
Maximum input current	12 A	Capacitor (C_1-C_2)	220 μF/450 V electrolyte
Initial efficiency	85.8%	Switches (S_1-S_4)	Si IRF260/IRF460
Switching frequency (f_s)	20 kHz	Diode (D_1-D_4)	Si STTH 6006 W

The results obtained from the observation of the inductor current using a current probe are presented in Figures 6 and 7. In the BCM graph, the blue waveform represents the inductor current, while the red waveform represents the stripe line, the switching signal. It can be observed that the shape of the inductor current in BCM is always continuous and momentarily touches zero. This pattern is similar in CCM, although the inductor current does not reach zero. In DCM, the red waveform represents the inductor current, while the blue waveform represents the switching signal. In DCM, there is a momentary zero current interval indicated by the black stripe line. This indicates that the converter has successfully operated in all operating modes.
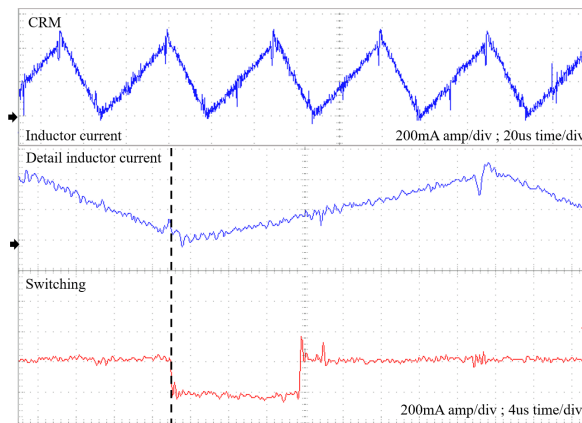
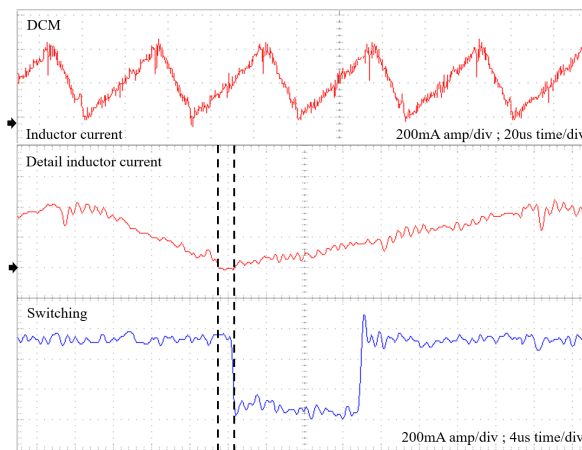Figure 6. Inductor current waveform at BCM

Figure 7. Inductor current waveform at DCM

4.2. Efficiency results

The experimental results are shown in the graph in Figure 8. It can be seen that with the converter parameters set according to Table 1, at a lower output current of 0.285 A, the converter operates in DCM condition, indicated by the inductor current waveform shown in Figure 7. The highest efficiency is achieved in this DCM condition, reaching 92.35% at an output power of 120.7 W. On the other hand, in the CCM condition, the efficiency only reaches a peak value of 91.61% at an output power of 131 W, which is close to the boundary mode. The lowest tested efficiency occurs at an output current of 0.605 A and an output power of 215.5 W, at 90.17% in CCM operation.

The efficiency trend observed is the highest in DCM, followed by BCM, and the lowest in CCM. In other words, efficiency decreases with increasing load/output current, indicating that the converter operates at higher power. The differences between experimental and calculated efficiencies are below 1%, indicating reasonably accurate results. The loss values are proportional to the increase in converter power. Additionally, in DCM, soft switching occurs, resulting in a drastic decrease in switch losses. This leads to a significant increase in efficiency between BCM and DCM, despite being close in output power. The calculations have been successfully verified through the experiments, and the calculations of each component's losses in the converter have been accurately approximated.

The highest efficiency achieved in the experiment is 92.35%. This value surpasses the optimization results in [22], which only reached 89.19%. This high efficiency was achieved by operating in DCM at low power. Furthermore, the selection of converter components, such as inductors, plays a crucial role in improving efficiency. To achieve even higher converter efficiency, components with lower conduction losses, such as

silicon carbide (SiC) or gallium nitride (GaN) switches and diodes, can be chosen. Additionally, the interconnection between converter components still uses bolted pins to facilitate component replacement during testing. In mass production, fabrication can be done by directly connecting components to the PCB using techniques such as dip soldering or robotic assembly in the factory. By addressing the losses in connections and component replacement, the converter efficiency is predicted to increase by 3-4%, reaching 96%.
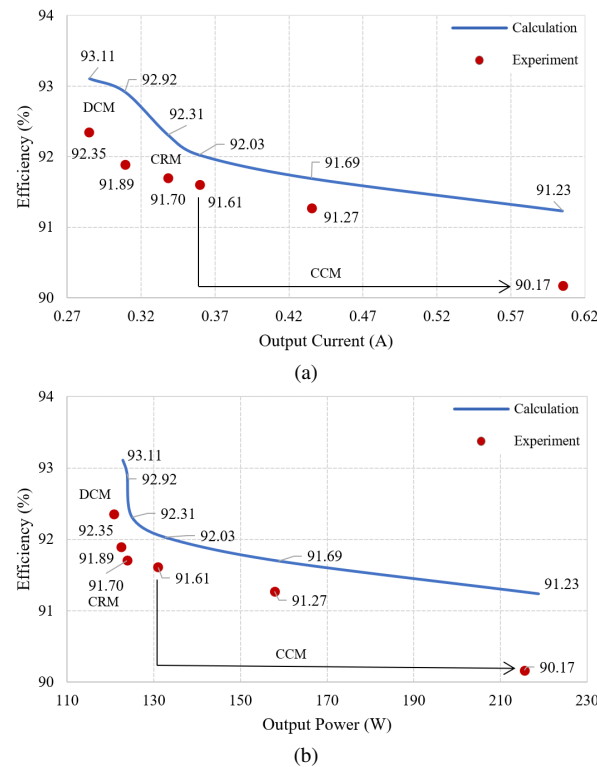
Figure 8. Calculation–experiment result: (a) efficiency vs. output current and (b) efficiency vs. output power

4.3. Losses fraction

The distribution of losses in the converter is presented in a pie chart as depicted in Figure 9. These results are obtained from the previously derived calculation formulas. There are conduction losses, which occur when current flows through components such as the inductor, diodes, and switches. The conduction losses in the inductor are further divided into AC losses and DC losses. Additionally, there are losses due to magnetic core losses in the inductor. Lastly, there are switching losses in the switches. These losses are presented in terms of power (W). The fraction of losses in the converter is analyzed for three different converter operations at closely spaced output powers: DCM at 120 W, BCM at 125 W, and CCM at 130 W. This is done to understand the relationship between the components that contribute significantly to the losses and the converter operating mode. As observed from the previous efficiency trends, the loss values are proportional to the increase in converter power, indicating higher losses in CCM. However, the fractions shown for each operating mode are different.

In DCM, the losses are dominated by the inductor core, accounting for 46% of the total losses, which amounts to 4.23 W. This occurs because the current ripple in the inductor increases slightly in DCM. As explained in section 2, the inductor core flux (B) is a function of Δi_L, so an increase in inductor current ripple leads to an increase in core losses. Additionally, the AC losses in the inductor in DCM are the highest among the modes, also due to the inductor current ripple. However, other losses, such as diode conduction, switch conduction, DC inductor losses, and switching losses, are relatively small. This is because the low-power operation results in lower current levels and, consequently, smaller losses compared to other modes. In particular, for switching losses, in the first-stage converter operating in DCM, soft switching occurs, resulting in nearly zero switching losses.

In BCM and CCM, the fraction of losses can be said to be similar, with inductor losses dominating the overall losses. However, these losses are not as significant as the core losses experienced in DCM. Additionally, losses due to diode conduction, switch conduction, DC inductor, and switching losses increase with the addition of load or an increase in output power, leading to an increased proportion of these losses in CCM. Generally, in the proposed converter, inductor losses dominate the overall losses, accounting for 62% of the total losses in DCM and 47% in CCM. Other significant losses include switch conduction losses and switching losses. The operation in DCM has been proven to significantly reduce switching losses, resulting in a considerable increase in efficiency at closely spaced output powers.
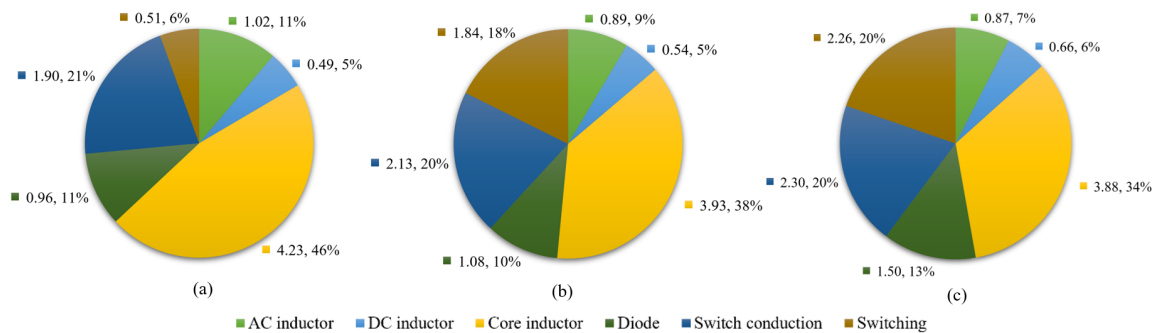
Figure 9. Losses fraction: (a) DCM, (b) BCM, and (c) CCM

5.   CONCLUSION

DCM operation provides the highest efficiency, reaching 92.2% at an output power of 120 W. In DCM, the core losses of the inductor increase, but the switch losses decrease drastically. At a low-power operation, overall losses are reduced. Efficiency decreases as the converter's power increases. However, both the calculated and experimental efficiency values of the converter remain above 90%. Furthermore, the output current of the converter becomes the determining factor for the operating mode of the first-stage converter, while the other parameters are kept constant, considering the flexibility to change other parameters and as a representation of grid load fluctuations.

For future development, components in the converter, such as switches and diodes, can be replaced with materials that have low resistance, such as silicon carbide (SiC) and gallium nitride (GaN). Additionally, the bolt pins can be removed to allow the components to be directly connected to the PCB, reducing losses in inter-component connections. Testing can be conducted over a wider power range, albeit requiring the replacement of some components.

AUTHOR CONTRIBUTIONS STATEMENT

This journal uses the Contributor Roles Taxonomy (CRediT) to recognize individual author contributions, reduce authorship disputes, and facilitate collaboration.

Name of Author	C	M	So	Va	Fo	I	R	D	O	E	Vi	Su	P	Fu
Arwindra Rizqiawan	✓			✓		✓				✓	✓	✓	✓	
Muhammad Farras Muzakki		✓	✓	✓	✓				✓					
Jihad Furqani					✓					✓		✓		

C	: **C**onceptualization	I	: **I**nvestigation	Vi	: **Vi**sualization
M	: **M**ethodology	R	: **R**esources	Su	: **Su**pervision
So	: **So**ftware	D	: **D**ata Curation	P	: **P**roject Administration
Va	: **Va**lidation	O	: Writing - **O**riginal Draft	Fu	: **Fu**nding Acquisition
Fo	: **Fo**rmal Analysis	E	: Writing - Review & **E**diting		

CONFLICT OF INTEREST STATEMENT

Authors state no conflict of interest.

DATA AVAILABILITY

The data that support the findings of this study are available from the corresponding author, [AR], upon reasonable request.

REFERENCES

[1] M. J. E. Alam, K. M. Muttaqi, and D. Sutanto, "A three-phase power flow approach for integrated 3-wire MV and 4-wire multigrounded LV networks with rooftop solar PV," *IEEE Transactions on Power Systems*, vol. 28, pp. 1728–1737, 2013, doi: 10.1109/TPWRS.2012.2222940.

[2] M. Hassan, S. Saha, and M. A. Haque, "A framework for the performance evaluation of household rooftop solar battery systems," *International Journal of Electrical Power and Energy Systems*, vol. 125, p. 106446, 2021, doi: 10.1016/j.ijepes.2020.106446.

[3] T. Araoye *et al.*, "Modeling and optimization of PV-diesel-biogas hybrid microgrid energy system for sustainability of electricity in rural area," *International Journal of Power Electronics and Drive Systems (IJPEDS)*, vol. 14, no. 3, pp. 1855–1864, Sep. 2023, doi: 10.11591/ijpeds.v14.i3.pp1855-1864.

[4] D. Aripriharta, D. Putri, M. Bagaskoro, W. Sujito, A. Wibawa, and S. Omar, "Techno economic analysis of PV pumping system for rural village in East Java," *e-Prime - Advances in Electrical Engineering, Electronics and Energy*, vol. 10, 100779, Dec. 2024, doi: 10.1016/j.prime.2024.100779.

[5] Ministry of Energy and Mineral Resources Directorate General of Electricity, "2021 Indonesia electrical statistics (in Bahasa: Statistik ketenagalistrikan tahun 2021)," Secretariat of the Directorate General of Electricity, 2021. [Online]. Available: https://gatrik.esdm.go.id/assets/uploads/download_index/files/6e4c6-statistik-2021-rev-2-.pdf. [Accessed: Sep. 20, 2023].

[6] H. Wirawan and Y. Gultom, "The effects of renewable energy-based village grid electrification on poverty reduction in remote areas: The case of Indonesia," *Energy for Sustainable Development*, vol. 62, pp. 186–194, Jun. 2021, doi: 10.1016/j.esd.2021.04.006.

[7] M. A. Setiawan, A. Abu-Siada, and F. Shahnia, "A new technique for simultaneous load current sharing and voltage regulation in DC microgrid," *IEEE Transactions on Industrial Informatics*, vol. 14, no. 4, pp. 1403–1414, 2018, doi: 10.1109/TII.2017.2761914.

[8] R. Khan, M. Nasir, and N. Schulz, "An optimal neighborhood energy sharing scheme applied to islanded DC microgrid for cooperative rural electrification," *IEEE Access*, vol. 11, pp. 116956–116966, 2023, doi: 10.1109/ACCESS.2023.3325769.

[9] N. Ayai *et al.*, "DC micro grid system," *SEI Technical Review*, no. 125, pp. 132–136, 2012.

[10] M. F. Elmorshedy, U. Subramaniam, J. S. Mohamed Ali, and D. Almakhles, "Energy management of hybrid DC microgrid with different levels of DC bus voltage for various load types," *Energies*, vol. 16, no. 14, p. 5438, 2023, doi: 10.3390/en16145438.

[11] M. Noritake *et al.*, "Experimental study of a 400 V class DC microgrid for commercial buildings," in *Proceedings of the 2015 9th International Conference on Power Electronics and ECCE Asia (ICPE-ECCE Asia)*, Seoul, Korea, Jun. 1–5, 2015, pp. 1730–1735, doi: 10.1109/ICPE.2015.7168011.

[12] C. R. Sullivan, J. J. Awerbuch, and A. M. Latham, "Decrease in photovoltaic power output from ripple: Simple general calculation and the effect of partial shading," *IEEE Transactions on Power Electronics*, vol. 28, no. 2, pp. 740–747, 2013, doi: 10.1109/TPEL.2012.2205162.

[13] G. Marsala and A. Ragusa, "Power losses analysis and efficiency evaluation of high boost converters for PV and fuel cell applications," in *Proceedings of 5th International Conference on Electric Utility Deregulation and Restructuring and Power Technologies*, Changsha, China, Mar. 2015, pp. 2201-2206, doi: 10.1109/DRPT.2015.7432620.

[14] R. Kiguchi and Y. Nishida, "Boost DC-DC converter cascade system for high boost-rate application," in *2018 International Conference on Smart Grid (icSmartGrid)*, Dec. 2018, doi: 10.1109/ISGWCP.2018.8634483.

[15] G. Gkizas, "Optimal robust control of a cascaded DC–DC boost converter," *Control Engineering Practice*, vol. 107, 104700, Feb. 2021, doi: 10.1016/j.conengprac.2020.104700.

[16] S. Hasanpour, Y. Siwakoti, and F. Blaabjerg, "Hybrid cascaded high step-up DC/DC converter with continuous input current for renewable energy applications," *IET Power Electronics*, vol. 13, no. 15, pp. 3487–3495, 2020, doi: 10.1049/iet-pel.2020.0544.

[17] A. I. Bratcu, I. Munteanu, S. Bacha, D. Picault, and B. Raison, "Cascaded DC–DC converter photovoltaic systems: Power optimization issues," *IEEE Transactions on Industrial Electronics*, vol. 58, no. 2, pp. 403–411, 2011, doi: 10.1109/TIE.2010.2043041.

[18] R. Stala *et al.*, "High-gain switched-capacitor DC-DC converter with low count of switches and low voltage stress of switches," *IEEE Access*, vol. 9, pp. 114267–114281, 2021, doi: 10.1109/ACCESS.2021.3104399.

[19] Y. Siwakoti and F. Blaabjerg, "Single switch nonisolated ultra-step-up DC-DC converter with an integrated coupled inductor for high boost applications," *IEEE Transactions on Power Electronics*, vol. 32, no. 11, pp. 8544–8558, 2017, doi: 10.1109/TPEL.2016.2646382.

[20] N. A. Elkhateb, J. Rahim, Selvaraj, and B. W. Williams, "DC-to-DC converter with low input current ripple for maximum photovoltaic power extraction," *IEEE Transactions on Industrial Electronics*, vol. 62, no. 4, 2015, doi: 10.1109/TIE.2014.2383999.

[21] M. Schuck and R. Pilawa-Podgurski, "Ripple minimization through harmonic elimination in asymmetric interleaved multiphase DC–DC converters," *IEEE Transactions on Power Electronics*, vol. 30, no. 12, pp. 7202–7214, Dec. 2015, doi: 10.1109/TPEL.2015.2393812.

[22] M. F. Muzakki, J. Furqani, and A. Rizqiawan, "High efficiency multiphase cascaded DC-DC boost converters with inductance optimization," in *Proceedings of The 5th International Conference of Power Engineering and Renewable Energy (ICPERE)*, Bandung, Indonesia, Nov. 2022, vol. 1, pp. 1-6, doi: 10.1109/ICPERE56870.2022.10037557.

[23] N. Boujelben, F. Masmoudi, M. Djemel, and N. Derbel, "Design and comparison of quadratic boost and double cascade boost converters with boost converter," in *Proceedings of 14th International Multi-Conference on Systems, Signals & Devices (SSD)*, Marrakesh, Morocco, Mar. 2017, pp. 245-252, doi: 10.1109/SSD.2017.8167022.

[24] M. Pahlavandust and M. R. Yazdani, "Single-switch boost DC-DC converter with zero-current-switching, high power density and low electromagnetic interference," *AEU - International Journal of Electronics and Communications*, vol. 121, p. 153229, 2020, doi: 10.1016/j.aeue.2020.153229.

[25] J. D. Navamani, M. L. Veena, A. Lavanya, and K. Vijayakumar, "Efficiency comparison of quadratic boost DC-DC converter in CCM and DCM," in *Proceedings of 2015 2nd International Conference on Electronics and Communication Systems (ICECS)*, Coimbatore, India, Feb. 2015, pp. 1156-1161, doi: 10.1109/ECS.2015.7124765.

[26] Micrometals Iron Powder Cores, "Micrometals powder core solutions T250-26," Division of Micrometals, Inc. [Online]. Available: https://datasheets.micrometals.com/T250-26-DataSheet.pdf. [Accessed: May 8, 2023].

[27] M. Sulthon, O. A. Damanik, A. Rizqiawan, and P. A. Dahono, "A new simplified cascaded boost converter for high ratio and low ripple application," in *2017 4th International Conference on Electric Vehicular Technology (ICEVT)*, Bali, Indonesia, Oct. 2017, pp. 117-124, doi: 10.1109/ICEVT.2017.8323545.

[28] T. Liu, T. Wong, and Z. J. Shen, "A survey on switching oscillations in power converters," *IEEE Journal of Emerging and Selected Topics in Power Electronics*, vol. 8, no. 1, pp. 893–908, 2020, doi: 10.1109/JESTPE.2019.2897764.

[29] N. Mohan, T. M. Undeland, and W. P. Robbins, *Power electronics: converters, applications, and design*, 3rd ed. USA: John Wiley & Sons, Inc., 2003.

[30] M. E. Başoğlu, "Comprehensive review on distributed maximum power point tracking: Submodule level and module level MPPT strategies," *Solar Energy*, vol. 241, pp. 85–108, 2022, doi: 10.1016/j.solener.2022.05.039.

BIOGRAPHIES OF AUTHORS

Arwindra Rizqiawan received the bachelor's and master's degrees from the Insititut Teknologi Bandung, Bandung, Indonesia, in 2006 and 2008, respectively, and a doctoral degree from the Shibaura Institute of Technology, Tokyo, Japan, in 2012, all in electrical engineering. He is currently serving as an faculty member of the School of Electrical Engineering and Informatics, Institut Teknologi Bandung. He is currently a Certified Professional Engineer in Indonesia with the Institution of Engineers Indonesia and ASEAN Engineer by ASEAN Engineering Register. His research interests include power engineering, power electronics, and renewable energy. He can be contacted at email: windra@itb.ac.id.

Muhammad Farras Muzakki received the bachelor's and master's degrees from the Insititut Teknologi Bandung, Bandung, Indonesia, in 2022 and 2023, respectively. His research interest includes power electronics converters and its application in renewable energy. He can be contacted at email: farrasmzki@gmail.com.

Jihad Furqani received the B.S. degree in electrical power engineering and the M.S. degree in electrical engineering from the Bandung Institute of Technology, in 2012 and 2013, respectively, and the Dr.Eng. degree in electrical and electronic engineering from the Tokyo Institute of Technology, in 2019. He has been studying multilevel and multiphase motor drive, noise reduction in switched reluctance motor, power electronic converter for renewable energy application, and electric motor for vehicle application. He was a Visiting Researcher with the University of Akron, in 2017, and a Visiting Lecture with the Tokyo Institute of Technology, in 2021. He received the IEEE Star Reviewer, in 2019. He can be contacted at email: j.furqani@yahoo.com.